

Observation of the pressure effect in simulations of droplets splashing on a dry surface.

A.M.P. Boelens,¹ A. Latka,² and J.J. de Pablo¹

¹*Institute for Molecular Engineering, University of Chicago,
5801 South Ellis Avenue, Chicago, Illinois 60637, USA*

²*Department of Physics, University of Chicago, 5720 South Ellis Avenue, Chicago, IL 60637, USA*
(Dated: September 17, 2018)

At atmospheric pressure, a drop of ethanol impacting on a solid surface produces a splash. Reducing the pressure suppresses this splash. The origin of the pressure effect is unknown and, until now, has not been reproduced in simulations. In this work the pressure effect is explored numerically by resolving the Navier-Stokes equations at a 10-nm resolution. In addition to reproducing numerous experimental observations, the simulations call the dewetting assumption for liquid sheet formation into question, and allow us to identify a previously unknown high-speed “rolling” contact line regime.

A wide variety of outcomes can occur when a liquid droplet hits a dry solid surface. Depending on impact velocity, surface tension, viscosity, ambient pressure, and surface roughness, either deposition, splashing, receding breakup, or a rebound of the droplet [1] can be observed. The effect of ambient pressure on the transition between the droplet-deposition regime and the splashing regime is particularly intriguing. While intuition suggests that pressure should have a stabilizing effect, it has been found that lowering, instead of increasing the ambient pressure, suppresses splashing. This phenomenon was first reported by Xu *et al.* [2] and, to date, attempts to capture it using numerical simulations have been unsuccessful [3–5].

One of the challenges of reproducing the so-called “pressure effect” is the multiscale nature of splashing. Length scales range from the contact line acting at nanometer length scales, to the characteristic length scale of the droplet itself, typically measuring tens of micrometers or larger. Time scales range from microseconds before impact, when deformation of the droplet leads to the entrapment of air under the droplet, forming the “central” air bubble [6–8], to milliseconds after impact, when fluid instabilities cause the liquid sheet that was ejected after impact to break up into many smaller droplets [9–12]. While past efforts have tried to identify a single splashing criterion [13, 14], all these length and time scales must be resolved or modeled in order to fully capture the physics of splashing.

In this Letter, by fully resolving the Navier-Stokes equations, we reproduce the pressure effect on splashing and, in doing so, reveal a number of features that help explain its origins. To achieve this, we perform calculations with spatial and temporal resolutions as high as 10nm and 10ps. These are length and time scales which are currently inaccessible to experiments, and such a high resolution can only be achieved by restricting our calculations to two dimensions. The main text of this Letter discusses splashing of an infinite cylinder on a dry surface. Results for axisymmetric droplets are provided in the Supplemental Material [16].

In addition to reproducing the pressure effect, simulations in both geometries also reproduce the formation of the central air bubble [6, 7], the formation and ejection of a liquid sheet [7, 10], and the contact line instability entraining gas bubbles at the liquid/gas interface [17]. Our simulations are also used to evaluate two recently developed theoretical models. One model proposes dewetting and the existence of a lift force [18] as the mechanisms driving liquid sheet formation and breakup. The other model attributes splashing to a “skating-like” motion of the droplet on a thin gas film and the deflection of liquid on the impact surface [8]. In our research we find that the liquid sheet is formed before dewetting is observed. However, there is merit to the skating droplet model. For breakup of the liquid sheet our results support the idea of a lift force, while deflection of the droplet on the surface does not seem to predict splashing. Several intriguing new findings are also revealed by our simulations. These include the appearance of two contact line regimes: a high-speed “rolling” regime, and a low-speed “sliding” regime. We also observe that three-dimensional instabilities are not strictly necessary to reproduce the pressure effect.

To facilitate the tracking of topological changes, a Volume of Fluid approach [15] is adopted in this work. In addition to the velocity and pressure fields, this method calculates the evolution of a phase-parameter field to track the liquid/gas interface. The Brackbill [19] surface tension model is used to calculate the Laplace pressure. On the wall, the Generalized Navier Boundary Condition (GNBC) is assumed [20] and, on the sides, air is allowed to flow in and out freely. As the initial condition for the phase parameter, the droplet is assumed to be completely spherical. The analytical expression for Stokes flow around a drop with internal circulation and matched stresses on the interface is used as the initial condition for the velocity field. This results in faster convergence compared to a uniform velocity field. The impact velocity is $v_0 = 5\text{ms}^{-1}$. More information about the equations, boundary conditions, and initial conditions used in this work can be found in the Supplemental Material [16].

The accurate description of the velocity and pressure fields upon impact requires that the deformation of the droplet be captured as it falls through the air. Initially, as the drop travels through the air, the resolution of the mesh can be relatively low and the simulation is run in a large box of $1 \times 5\text{mm}$ at a resolution of 320×1600 grid cells. Towards the wall, the mesh is refined six times. Each refinement divides a grid cell into four, giving a smallest grid size of 50nm . Once the droplet is sufficiently close to the wall, the simulation results in the lower part of the large simulation box are saved and reinitialized within a small box of $1 \times 0.5\text{mm}$. To capture the details at the contact line this small box has a resolution of 320×160 grid cells, and the mesh is refined eight times towards the wall. This results in a minimum grid size of about 10nm . From a computational point of view, this is the smallest feasible mesh size that we can adopt for this system. Complete convergence would require a grid size below the slip length, which is approximately 1nm and is beyond the reach of our computational resources. Nevertheless, at a grid size of 10nm the necessary physics of splashing are already present, and we expect the main observations of our simulations to be qualitatively correct. The width of both boxes is chosen to be large enough for the splash to occur within their confines.

The fluids considered in our simulations are ethanol, for the liquid phase, and air, for the gas phase. This combination has been used in experiments [2], and has the advantage of showing an early splash, i.e. shortly after impact. In experiments, the pressure effect is observed at moderately reduced gas pressures [2]. We therefore assume the dynamic viscosity of the air to be constant, while the density and the kinematic viscosity change as pressure is reduced [21]. To reduce memory requirements, we consider a two-dimensional droplet with a diameter of $300\mu\text{m}$ (as opposed to the 3mm droplets used in the experiments of Xu *et al.* [2]).

Fig. 1 shows a time series of the pressure effect. The top half shows two images of droplet impact and liquid sheet ejection on a completely wetting surface at ambient pressure, $p_0 = 100\text{kPa}$. The first frame, Fig. 1a, shows the droplet right before impact. At this moment, as the droplet approaches the wall, gas pressure builds up at the stagnation point to about $p = 400\text{kPa}$. This causes the droplet to deform, and an air pocket in the shape of a spherical dome appears underneath it. As the gap between the surface and the droplet closes, air gets squeezed out and reaches velocities of up to $|\vec{v}| = 100\text{m s}^{-1}$. When the liquid eventually touches the wall, a small amount of air is permanently trapped, forming the central air bubble with a diameter of about $d = 6\mu\text{m}$ [6–8].

Fig. 1b shows the ejection of a liquid sheet. The sheet gets ejected with a velocity of about $|\vec{v}_{s,0}| = 54\text{m s}^{-1}$. The liquid sheet forms at both atmospheric, $p_0 = 100\text{kPa}$, and reduced pressure, $p_0 = 1\text{kPa}$. However, at atmospheric pressure the sheet gets lifted and

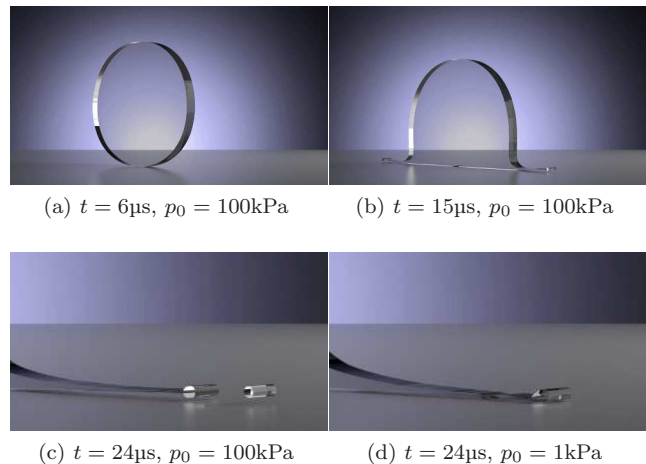


Figure 1. Time series of the impact of a cross section of a cylinder on a dry surface. The top frames show simulation results for atmospheric pressure. The bottom frames show 3 times magnified images of liquid sheet breakup at atmospheric pressure, and no breakup at reduced pressure.

breaks up into smaller droplets; in contrast, at reduced pressure it stays close to the surface and remains in one piece. The reduced ambient pressure used in the simulations was deliberately chosen significantly below the experimentally observed threshold pressure, to ensure that the simulations were performed well into the suppressed splashing regime. Fig. 1c shows a magnified image of the liquid sheet as it breaks up into smaller droplets, at atmospheric pressure. The droplet that breaks off has a size of $d = 7\mu\text{m}$. Fig. 1d shows a snapshot taken at the same time, but at a reduced pressure. It can be observed that instead of breaking up, the liquid sheet stays in one piece and splashing is suppressed by decreasing the ambient pressure. More detailed information on the thickness profiles of both the gas layer and the liquid sheet can be found in the Supplemental Material [16].

Before looking into more details, it is of interest to point out a couple of features of our calculations. To reduce the number of variables, both the liquid and gas phases are assumed to be incompressible; this indicates, as was originally shown by Driscoll and Nagel [7], that a shock wave cannot be responsible for liquid sheet formation. As was also demonstrated experimentally by Bischofberger *et al.* [22], vortex formation in the gas phase upon impact is not necessary for splashing. Although the vortices are not resolved in our simulations, the effect of pressure is still captured. Lastly, the break up of the liquid sheet is thought to be caused by either a Plateau-Rayleigh instability, or a Rayleigh-Taylor instability [12]. Although a Plateau-Rayleigh instability can play a role in three-dimensional splashing, since in these two-dimensional simulations breakup is still observed, it can be concluded that such an instability is not necessary

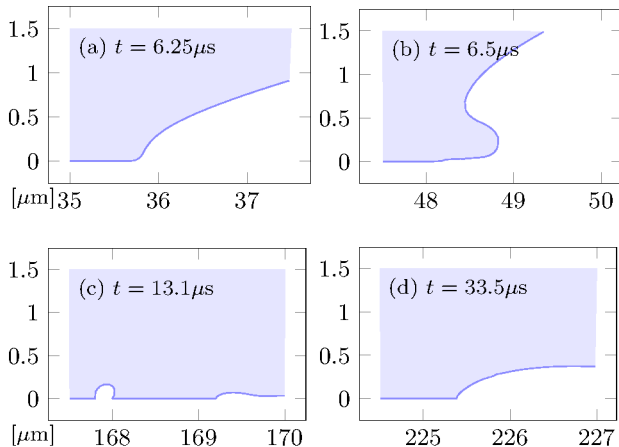


Figure 2. Time series of the droplet interface showing the evolution of the contact line at atmospheric pressure. Light blue represents the liquid phase. The vertical axis shows the distance normal to the surface and the horizontal axis shows the distance parallel to the surface relative to the center of the droplet. Both axes are in μm .

to observe the splashing effect.

Perhaps the more important aspect of our simulations is that they provide access to length and time scales that are not easily observed in experiments. An example of this can be seen in Fig. 2, which presents a zoomed-in time series of the liquid/gas interface at the contact line. These snapshots are taken at atmospheric pressure, from the moment just after impact until the point when the edge of the droplet is about to leave the simulation box. Drop impact is defined as the moment the value of the phase parameter, $\alpha = 0.5$, is first detected on the wall. This happens at $t = 6.2\mu\text{s}$. Fig. 2a shows the contact line just after impact and right before a liquid sheet forms at $t = 6.33\mu\text{s}$. Once the liquid sheet forms, it is ejected right away, which can be seen in Fig. 2b. A feature revealed by experiments [7] and used in theory as a criterion for liquid sheet ejection [18] is contact line dewetting, and the associated gas bubble entrainment at the contact line. This phenomenon can be appreciated in Fig. 2c, which at $r \approx 168\mu\text{m}$ shows a gas bubble that formed when the contact line became unstable, and the liquid in front of the contact line touched down on the surface. The first touch-down event is observed at $t = 7.33\mu\text{s}$, and at $t = 14.4\mu\text{s}$ the contact line stabilizes again. This can be seen in Fig. 2d. It is interesting to note that the contact line becomes unstable a full $1\mu\text{s}$ after liquid sheet formation. Since initially a small gas bubble gets entrained about every $0.5\mu\text{s}$, this suggests that the liquid sheet forms before the contact line becomes unstable, which is in disagreement with the dewetting assumption of Riboux and Gordillo [18].

In addition to these findings, Fig. 2 provides another new insight into the onset of splashing, which can be

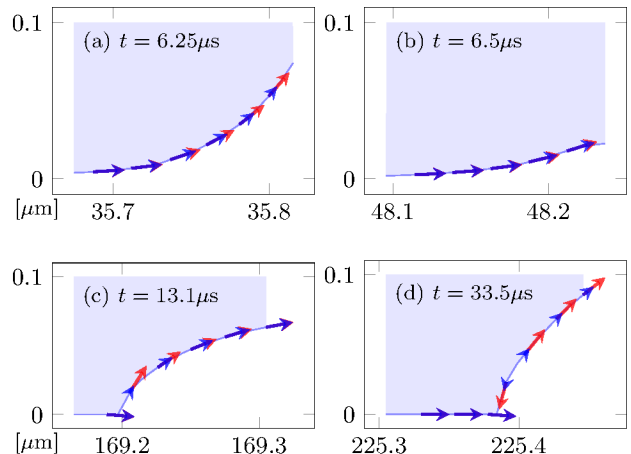


Figure 3. Time series of the droplet interface, and non-dimensional interface velocity, \hat{v}_i , showing the evolution of the contact line at atmospheric pressure. This time series is zoomed in 15 times compared to Fig. 2. Unit vector (\rightarrow), non-dimensional interface velocity (\rightarrow). Light blue represents the liquid phase, and the axis are in μm .

appreciated when we zoom into the contact line a bit further. In Fig. 3 this zoomed-in time series of the contact line and non-dimensional interface velocity, \hat{v}_i , is shown at atmospheric pressure. While in the last two frames a normal low-speed contact line can be observed, the contact line in the first two frames shows a strongly curved interface instead, which continues under the droplet. This means that there is either a very thin gas layer under the droplet that cannot be resolved at the current resolution, or that, down to molecular length scales, the interface is touching the wall. The continuation of the interface under the droplet could be the equivalent of the short-lived thin film of air that has been observed under splashing droplets in experiments [23]. It also seems consistent with the theoretical prediction that a droplet skates on a thin air film before liquid sheet ejection [8]. The fact that the interface only continues under the droplet for a length of about $l = 5\mu\text{m}$, and is short lived, could explain why it was not detected in past interference experiments [7].

To gain more insight into the behavior of the curved interface at the contact line, we now focus on the non-dimensional interface velocity, \hat{v}_i . To calculate the non-dimensional interface velocity, the velocity of the interface, \vec{v}_i , is decomposed into a component tangential to the interface, $\vec{v}_{i,t}$, and a component in the direction of the translation of the interface, $\vec{v}_{i,r}$. The tangential velocity is then made non-dimensional according to: $\hat{v}_i = \vec{v}_{i,t}/|\vec{v}_{i,r}|$. When an object is undergoing a purely “rolling” motion, e.g. a cylinder rolling over a surface, the magnitude of the tangential component of the interface velocity is equal to the magnitude of the

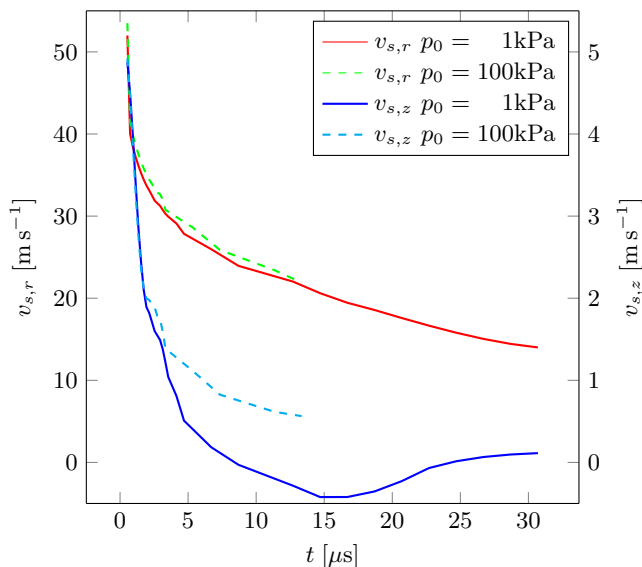


Figure 4. The radial, $v_{s,r}$, and vertical, $v_{s,z}$, velocity components of the liquid sheet ejected from the droplet as function of time since impact. The theoretical prediction is; $v_{s,r,M} \approx 60 \text{ m s}^{-1}$.

translational component, and the magnitude of the non-dimensional interface velocity is unity. When the tangential and translational velocities are not equal, and the object is (partly) slipping, the non-dimensional interface velocity is no longer unity. When comparing the non-dimensional interface velocity vector field with the unit vector field, it can be observed that at early times the non-dimensional interface velocity is very close to one, and thus the interface rolls over the surface at a high speed, like a caterpillar track. At later times, the non-dimensional interface velocity is much smaller than unity, indicating that, at low velocities, contact line movement is dominated by slip. The introduction of a rolling contact line regime also makes for a new prediction. When the contact line is in the rolling regime, the contact line should behave in exactly the same manner on wetting and non-wetting surfaces. Therefore, in this regime, liquid-sheet formation is predicted to be independent of the wetting properties of the surface. This makes splashing of droplets on a dry surface different from plunging objects into a liquid. In that case the splash strongly depends on the wetting properties of the object's surface [24].

The above results call the dewetting assumption into question. We now address the validity of the skating drop assumption. In Fig. 4 we zoom back out from the contact line and look at the radial and vertical liquid sheet velocities to compare them with theoretical predictions. The predictions for the liquid sheet ejection velocities by Riboux and Gordillo [18] only apply to axisymmetric geometries, and are discussed in the Supplemental Material [16]. The predictions of Mandre and Brenner [8] for planar geometries are discussed here in the main text.

Using the equations shown in the Supplemental Material [16], one can calculate that the skating droplet theory of Mandre and Brenner predicts a liquid sheet ejection velocity of $v_{s,r,M} \approx 60 \text{ m s}^{-1}$. Looking at Fig. 4, it can be seen that the ejection velocity observed in simulations is about $v_{s,r} \approx 54 \text{ m s}^{-1}$. This is close to the predicted value, and confirms the merit of the skating droplet assumption.

In order to arrive at a criterion for whether a droplet will splash or not, a parameter $\beta = v_{h_t,z}/v_{tc}$ can be defined [18], where $v_{h_t,z}$ is the vertical velocity of the liquid sheet when it has risen a characteristic height of h_t , and v_{tc} is the Taylor-Culick velocity. Looking at the curves for v_s , it can be seen that both the vertical and radial ejection velocities are very similar for both pressures, and that at early times the value of β would not be able to predict splashing because of matching vertical velocities at different pressures. This is confirmed by the axisymmetric results included in the Supplemental Material [16]. On the other hand, the fact that the liquid sheet velocities start to differ later on, does support the idea of a lift force acting on the liquid sheet. Other literature predictions suggest [8] that splashing depends on the deflection of the droplet on the surface. Since both droplets touch the surface, deflection would predict both droplets to splash, which is not the case. Lastly, these simulations support the idea that splashing consists of multiple stages where a sheet must form first, which then gets broken up or not depending on conditions.

In summary, the high-resolution numerical simulations of splashing ethanol droplets presented here appear to describe the so-called ‘‘pressure effect’’ with considerable fidelity. The formation of the experimentally observed central air bubble, air bubble entrainment at the contact line, and liquid sheet formation are all reproduced. The simulations reported here have allowed us to address recent theoretical predictions, and determine that for liquid sheet formation the dewetting assumption does not seem to hold, while the results are in better agreement with the so-called skating droplet assumption. For the vertical acceleration of the liquid sheet and its subsequent breakup, the β parameter defined by Riboux and Gordillo does not appear to offer predictive power, while the idea of liquid sheet acceleration by a lift force is supported. Droplet deflection on the surface does not seem to be able to predict splashing. Simulations have also allowed us to identify two distinct contact line regimes, at high and low liquid velocities. At high velocities the contact line moves in a rolling fashion, while at low speeds the contact line slips on the surface, thereby predicting the independence of liquid sheet formation on the wetting properties of the surface. Last, but not least, it is found that three-dimensional fluid instabilities, like the Plateau-Rayleigh instability are not needed to observe the pressure effect.

The authors would like to thank Sidney Nagel, Michelle

Driscoll, Casey Stevens, and Irmgard Bischofberger for many fruitful discussions of the simulation results.

-
- [1] A. L. Yarin, *Annu. Rev. Fluid Mech.* **38**, 159 (2006).
- [2] L. Xu, W. W. Zhang, and S. R. Nagel, *Phys. Rev. Lett.* **94**, 184505 (2005).
- [3] L. Duchemin and C. Josserand, *Phys. Fluids* **23**, 091701 (2011).
- [4] G. Taura and M. Matsumoto, *J. Fluid. Sci. Tech.* **5**, 207 (2010).
- [5] J. Koplik and R. Zhang, *Phys. Fluids* **25**, 022003 (2013).
- [6] S. Chandra and C. T. Avedisian, *Proc. R. Soc. London, Ser. A*, 13 (1991).
- [7] M. M. Driscoll and S. R. Nagel, *Phys. Rev. Lett.* **107**, 154502 (2011).
- [8] S. Mandre and M. P. Brenner, *J. Fluid Mech.* **690**, 148 (2012).
- [9] R. F. Allen, *J. Colloid Interface Sci.* **51**, 350 (1975).
- [10] J. E. Field, J. P. Dear, and J. E. Ogren, *J. Appl. Phys.* **65**, 533 (1989).
- [11] O. Tammisola, A. Sasaki, F. Lundell, M. Matsubara, and L. D. Söderberg, *J. Fluid Mech.* **672**, 5 (2011).
- [12] G. Agbaglah, C. Josserand, and S. Zaleski, *Phys. Fluids* **25**, 022103 (2013).
- [13] C. D. Stow and M. G. Hadfield, *Proc. R. Soc. London, Ser. A* **373**, 419 (1981).
- [14] C. S. Stevens, *Europhys. Lett.* **106**, 24001 (2014).
- [15] C. W. Hirt and B. D. Nichols, *J. Comput. Phys.* **39**, 201 (1981).
- [16] Supplemental Materials available online at: <http://arxiv.org>.
- [17] M. M. Driscoll, C. S. Stevens, and S. R. Nagel, *Phys. Rev. E* **82**, 036302 (2010).
- [18] G. Riboux and J. M. Gordillo, *Phys. Rev. Lett.* **113**, 024507 (2014).
- [19] J. U. Brackbill, D. B. Kothe, and C. Zemach, *J. Comput. Phys.* **100**, 335 (1992).
- [20] T. Qian, X.-P. Wang, and P. Sheng, *Phys. Rev. E* **68**, 016306 (2003).
- [21] K. Kadoya, N. Matsunaga, and A. Nagashima, *J. Phys. Chem. Ref. Data* **14**, 947 (1985).
- [22] I. Bischofberger, K. W. Mauser, and S. R. Nagel, *Phys. Fluids* **25**, 091110 (2013).
- [23] J. M. Kolinski, S. M. Rubinstein, S. Mandre, M. P. Brenner, D. A. Weitz, and L. Mahadevan, *Phys. Rev. Lett.* **108**, 074503 (2012).
- [24] C. Duez, C. Ybert, C. Clanet, and L. Bocquet, *Nature Phys.* **3**, 180 (2007).

Supplemental material to: Observation of the pressure effect in simulations of droplets splashing on a dry surface.

A.M.P. Boelens,¹ A. Latka,² and J.J. de Pablo¹

¹*Institute for Molecular Engineering, University of Chicago,
5801 South Ellis Avenue, Chicago, Illinois 60637, USA*

²*Department of Physics, University of Chicago, 5720 South Ellis Avenue, Chicago, IL 60637, USA*
(Dated: September 17, 2018)

This document contains supplemental information about the used numerical method, gas film thickness, and a comparison with theory.

Volume Of Fluid method

To be able to completely simulate the breakup of a splashing droplet, the Volume Of Fluid (VOF) method is used, which was first developed by Hirt and Nichols [1]. The VOF approach evolves around the definition of a phase parameter α with the following properties:

$$\alpha = \begin{cases} 0 & \text{in gas phase} \\ (0, 1) & \text{on interface} \\ 1 & \text{in liquid phase} \end{cases} \quad (1)$$

The evolution of α is calculated using the following transport equation:

$$\frac{\partial \alpha}{\partial t} + \nabla \cdot (\alpha \vec{v}) + \nabla \cdot (\alpha(1-\alpha) \vec{v}_{lg}) = 0, \quad (2)$$

where \vec{v} is the phase averaged velocity, and \vec{v}_{lg} is the velocity difference between the liquid and the gas phase. This equation is equivalent to a material derivative, but rewritten to minimize numerical diffusion [2].

The phase parameter is used to calculate the phase averaged density, ρ , velocity, \vec{v} , and viscosity, μ , which are used in the momentum balance:

$$\frac{\partial \rho \vec{v}}{\partial t} + \nabla \cdot (\rho \vec{v} \otimes \vec{v}) = -\nabla p + \nabla \cdot (\mu \nabla \vec{v}) + \rho \vec{g} - \vec{f}, \quad (3)$$

and the continuity equation:

$$\nabla \cdot \vec{v} = 0. \quad (4)$$

In the above equations t is time, p is pressure, g is gravity, \vec{f} is any body force, like the surface tension force, and \otimes is the dyadic product. To complete the VOF model, an expression is needed to calculate the surface tension force \vec{f}_{st} , and the initial and boundary conditions need to be chosen. The surface tension force is calculated using the expression:

$$\vec{f}_{st} = \sigma_{st} \kappa \nabla \alpha \quad (5)$$

where σ_{st} is the surface tension coefficient, and κ is the curvature of the interface. This expression for the surface tension force was first derived by Brackbill *et al.* [3].

The computational domain has two different kinds of boundary conditions for each variable; on the bottom there is the impact wall, and on the sides and top there are boundary conditions which allow for the in and out flow of gas. As boundary condition for α on the impact wall the Generalized Navier Boundary Condition is used [4, 5]. With this boundary condition the dynamic contact angle is allowed to vary freely, but a restoring line-tension force is applied at the contact line whenever the dynamic angle deviates from the equilibrium contact angle. This restoring force is an additional source term in the Navier-Stokes equations, and has the following form:

$$\vec{f}_{lt} = C \frac{\sigma_{st}}{h} (\cos \theta - \cos \theta_0) \nabla_{2D} \alpha \quad (6)$$

This force is applied on the liquid-gas interface in the first grid cells next to the wall. In the above equation $C = 4\alpha(1-\alpha)$ is a pre-factor to ensure the restoring force is only acting on the contact line, σ_{st} is the surface tension coefficient, $h = V/A$, is the mesh height, with A the surface area of the wall in a grid cell, and V its volume, θ is the dynamic contact angle, θ_0 is the equilibrium contact angle, and $\nabla_{2D} \alpha$ is the gradient of α on the wall. More information on the derivation and validation of this boundary condition can be found in Ref. [6]. On the wall the velocity obeys the Navier-slip boundary condition with a slip-length of $\lambda_N = 1\text{nm}$. For mass conservation, the boundary condition for the pressure enforces both a zero flux and a zero second derivative of the pressure normal to the wall.

On the other sides of the simulation box the phase parameter, α , obeys a Dirichlet fixed-value boundary condition for inflow and a zero-gradient Neumann boundary condition for outflow. The Dirichlet fixed value is set to zero, which is equivalent to only allowing gas to flow in. For each grid cell next to a side wall the local inflow velocity is calculated from the wall-face normal component of the velocity vector associated with the center of that specific grid cell. The boundary condition for the outflow velocity is a zero-gradient Neumann boundary condition. The total pressure p_0 on the side walls is kept constant according to a simplified Bernoulli's equation:

$$p_0 = p + \frac{1}{2} \rho |\vec{v}|^2. \quad (7)$$

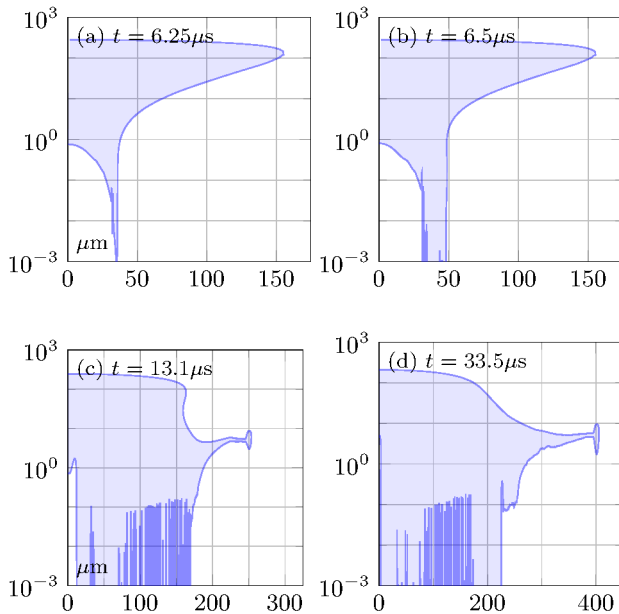


Figure 1. Time series of the droplet interface with the vertical axis plotted on a logarithmic scale. The axis are in μm .

In this boundary condition the gas is assumed inviscid, and when the gas inflow velocity, \vec{v} , changes, the pressure, p , changes accordingly.

As mentioned in the main text, to allow the droplet to equilibrate with the gas flow around it the droplet first falls through a large simulation box at a lower resolution. As initial condition for α , the droplet is assumed to be a perfect sphere, with its center of mass located at a height of 4.5mm . To reach faster convergence of the gas velocity field, Stokes flow is assumed both inside and outside the droplet as initial condition, and stresses are matched on the interface [7]. The pressure field does not need to be initialized and develops as the simulation progresses. The above equations are solved using the VOF solver of the OpenFOAM Finite Volume toolbox [8].

Air film thickness

Considering how small the features at the contact line are, it would be a valid question to ask whether the continuity approximation is valid in these simulations. To be able to analyze the thickness of the gas film under the droplet, Fig. 1 shows a time series of the contour of the droplet at atmospheric pressure with the vertical axis plotted on a logarithmic scale. Since the vertical axis cannot go to zero, it is cut off at $10^{-3}\mu\text{m}$, and the center of the drop corresponds to the vertical axis. Fig. 1a shows the droplet right after impact with the central air dome clearly visible. Initially the bubble is slightly under $1\mu\text{m}$ high, and about $30\mu\text{m}$ wide. The vertical lines or

peaks under the droplet are small air bubbles which were trapped on impact. The next figure shows the droplet right after a liquid sheet is ejected. From the main text it is known that the liquid sheet ejects at a height of around $0.5\mu\text{m}$, and careful inspection of the contour line $50\mu\text{m}$ away from the center does indeed show a deflection point at this height. The third frame shows the droplet in the unstable contact line regime. The vertical lines behind the contact line are small air bubbles which were entrained by the moving contact line. Also, it can be observed how the contact line of the central air bubble is moving toward the center. The gas layer under the liquid sheet is on the order of several microns thick. The last figure, Fig. 1d, shows the droplet with a stable contact line. There are no longer droplets being trapped right behind the contact line. Instead, there is just one cavity present at the contact line with a height of a little under $1\mu\text{m}$. The gas film right after the cavity has a thickness of about $0.1\mu\text{m}$, and increases again to several microns towards the rim of the liquid sheet.

To put the above numbers in perspective they need to be compared to the mean free path of air. At room temperature and atmospheric pressure the mean free path is around $\lambda \approx 70\text{nm}$ [9]. The typical thickness of the gas layer is several microns, so the continuity approximation should be valid for these simulations. Since the mean free path scales with the kinematic viscosity, at the reduced pressure the mean free path is about $\lambda \approx 7\mu\text{m}$, which is about the same height as the typical thickness of the gas layer. This means that at reduced pressure the validity of the continuum approximation is pushed to its limits. However, in experiments the splashing effect is observed already around an ambient gas pressure of $p_0 \approx 20\text{kPa}$ [10], which means a mean free path of $\lambda \approx 350\text{nm}$. Since, in this work we have not truly taken the properties of air at $p_0 = 1\text{kPa}$, but instead have exaggerated the properties of air at $p_0 = 20\text{kPa}$ (i.e. the assumption of constant dynamic viscosity), we expect that these simulations are representative of the behavior of the gas film in experiments.

Theoretical models

Two theories predicting splashing are the models developed by Mandre and Brenner [11] and Riboux and Gordillo [12]. This section compares the results of the simulations to these models. Table I shows an overview of the different simulations that are used in this comparison. Case 1 is the same set of simulations that is presented in the main text, and represents the splashing of an infinite cylinder at $v_0 = 5\text{m s}^{-1}$. Case 2 is a set of axisymmetric simulations of a droplet impact at $v_0 = 5\text{m s}^{-1}$, and case 3 is a set of axisymmetric simulations of a droplet impact at $v_0 = 10\text{m s}^{-1}$. For the axisymmetric simulations, the impact velocity of $v_0 = 5\text{m s}^{-1}$ is not large enough

Table I. Parameters of different simulation cases and their results.

	p_0 [kPa]	v_0 [m s ⁻¹]	Geometry	Splash
Case 1a	1	5	non-axisym	no
Case 1b	100	5	non-axisym	yes
Case 2a	1	5	axisym	no
Case 2b	100	5	axisym	no
Case 3a	1	10	axisym	no
Case 3b	100	10	axisym	yes

Table II. Non-dimensional numbers of the different cases.

	St	Re	We	Oh
Case 1	0.000025	493	132	0.0233
Case 2	0.000025	493	132	0.0233
Case 3	0.000013	986	528	0.0233

to cause a splash at $p_0 = 100\text{kPa}$, but the impact velocity of $v_0 = 10\text{m s}^{-1}$ is. All presented results are non-dimensionalized with the impact velocity, v_0 , and the droplet radius, r_0 . Mandre and Brenner define impact time, t_0^M , as the moment that a non-deformed droplet would have hit the surface. In our analysis, we took this to be the moment when the top of the droplet is one diameter away from the wall. Impact time for Riboux and Gordillo, t_0^R , is defined as the moment that the phase parameter value $\alpha = 0.5$ is first detected on the wall. Liquid sheet ejection time, t_e , is defined as the moment a local maximum can first be detected in the width of the droplet close to the wall. This local maximum is the beginning of a liquid sheet. Ejection time is calculated relative to the moment of impact. When t_0^M is used to calculate the ejection time from our simulation results it is called, t_e^M . When t_0^R is used the ejection time is labeled t_e^R . Because the theory of Mandre and Brenner was developed for a 2D planar geometry, it will only be compared to case 1. The theory of Riboux and Gordillo was developed for axisymmetric geometries, and will be compared to cases 2 and 3.

The relevant non-dimensional numbers in this system are:

$$\text{St} = \frac{\mu_g}{\rho_l v_0 r_0}, \quad \text{We} = \frac{\rho_l v_0^2 r_0}{\sigma},$$

$$\text{Re} = \frac{\rho_l v_0 r_0}{\mu_l}, \quad \text{and} \quad \text{Oh} = \frac{\sqrt{\text{We}}}{\text{Re}},$$

where St is the inverse Stokes number, Re is the Reynolds number, We is the Weber number, and Oh is the Ohnesorge number. Table II shows the values of these numbers using the following parameters: $\rho_l = 789\text{kg m}^{-3}$, $\mu_l = 1.20 \times 10^{-3}\text{Pa s}$, $\rho_g = 0.01\text{kg m}^{-3}$ at $p_0 = 1\text{kPa}$, $\rho_g = 1.00\text{kg m}^{-3}$ at $p_0 = 100\text{kPa}$, $\mu_g = 1.48 \times 10^{-5}\text{Pa s}$, $\sigma = 0.02239\text{J m}^{-2}$, and $r_0 = 150\mu\text{m}$. These numbers

suggest that in our simulations impact is dominated by the inertia of the fluid.

Table III. Comparison of simulation results with predictions of the model by Mandre and Brenner [11]. The table shows ejection times, ejection velocities, and breakup times of the liquid sheet.

	$t_{e,M}$	t_e^M	t_e^R	$v_{e,M}$	v_e	t_b
Case 1a	0.00650	0.092	0.00167	11.6	10.4	—
Case 1b	0.00650	0.134	0.00333	11.6	10.7	0.292

Mandre and Brenner [11] calculate the non-dimensional liquid sheet ejection time and velocity with the following equations:

$$t_{e,M} = 7.6\text{St}^{2/3} \quad \text{and} \quad v_{e,M} = 0.34\text{St}^{-1/3}, \quad (8)$$

which gives the results shown in Table III. Although the ejection times do not match very well, the sheet ejection velocities are very close. The differences in the ejection time can stem from the fact that Mandre and Brenner have a perfectly circular drop right before impact while in our simulations our drop deforms as it falls through the air before impact. When instead of t_0^M , t_0^R is taken as the moment of impact to calculate t_e^R , the predicted times are of the same order as the ejection times found in our simulations. Another factor that can contribute to a difference in both ejection times and ejection velocities is the assumption of inviscid flow by Mandre and Brenner.

Table IV. Comparison of simulation results with predictions of the model by Riboux and Gordillo [12]. The table shows ejection times, ejection velocities, splashing criterion, and breakup times of the liquid sheet.

	$t_{e,R}$	t_e^R	$v_{e,R}$	v_e	β_R	β	t_b
Case 2a	0.0539	0.0100	3.73	5.95	0.068	0.501	—
Case 2b	0.0539	0.0100	3.73	6.02	0.527	0.448	—
Case 3a	0.0317	0.0000	4.87	7.05	0.075	0.523	—
Case 3b	0.0317	0.0067	4.87	7.65	0.649	0.557	0.800

In Table IV the theoretical predictions of Riboux and Gordillo [12] are shown. To calculate sheet ejection times the following equation is used:

$$c_1 \text{Re}^{-1} t_{e,R}^{-1/2} + \text{Re}^{-2} \text{Oh}^{-2} = c^2 t_{e,R}^{3/2} \quad (9)$$

where c_1 and c are two constants with the values $c_1 = \sqrt{3}/2$ and $c = 1.1$. Once the ejection time is known the ejection velocity is calculated with:

$$v_{e,R} = \frac{\sqrt{3}}{2} t_{e,R}^{-1/2}. \quad (10)$$

In addition, Riboux and Gordillo derive the parameter β to predict splashing. β is calculated from our simulations

using:

$$\beta = \frac{v_{h_t,z} v_0}{\sqrt{2\sigma/(\rho_l h_t r_0)}} \quad (11)$$

where $v_{h_t,z}$ is the vertical velocity of the liquid sheet when it has risen a characteristic height of:

$$h_t = \frac{\sqrt{12}}{\pi} t_{e,R}^{3/2} \quad (12)$$

For case 2a this is the vertical velocity at $t = 0.18$, for case 2b at $t = 0.20$, for case 3a at $t = 0.17$, and for case 3b at $t = 0.26$. The theoretical value β_R is calculated using the equation:

$$\beta_R = \left(\frac{K_l \mu_g (v_{e,R} v_0) + K_u \rho_g (v_{e,R} v_0)^2 (h_t r_0)}{2\sigma} \right)^{1/2} \quad (13)$$

with:

$$K_l = -\frac{6}{\tan^2(\alpha)} \left[\ln\left(16 \frac{l_g}{h_t r_0}\right) - \ln\left(1 + 16 \frac{l_g}{h_t r_0}\right) \right], \quad (14)$$

and:

$$K_u = 0.3. \quad (15)$$

In the above equation $\alpha = 20/180 \pi^\circ$, and $l_g = 1.2\lambda$, the slip length of the gas. $\lambda = \lambda_0 (p_{\text{atm}}/p_0)$ with $\lambda_0 = 65\text{nm}$ the mean free path of air at room temperature and atmospheric pressure, $p_{\text{atm}} = 100\text{kPa}$. Comparing the results for ejection times found in simulations and theory, the theoretical values seem to be systematically over-predicted by about 5 times. Liquid sheet ejection velocities are under-predicted, but by about 1.5 times. Both phenomena could be due to the fact that liquid sheet formation is observed before dewetting, which is taken as the condition for liquid sheet formation by Riboux and Gordillo. Comparing the two columns β and β_R , it can be observed that theory predicts about an order difference between normal and reduced pressure cases. However, the values calculated from the simulations show similar values for β for all cases. This suggests that β is not able to predict splashing for these simulations. The last column shows the breakup time of the liquid sheet for completeness.

While in these simulations the value of β does not seem to be a good splashing criterion, the individual velocity components, shown in Fig. 2 and Fig. 3, do suggest that a lift force could be responsible for the breakup of a liquid sheet. Initial vertical ejection velocities are very similar between normal and reduced pressure cases. However, at later times, when a lift force could have started acting on the liquid sheet, the velocities start to diverge. Comparing different geometries it can be observed that although ejection velocities decrease going from the cylinder to the axisymmetric geometry, all trends are the same.

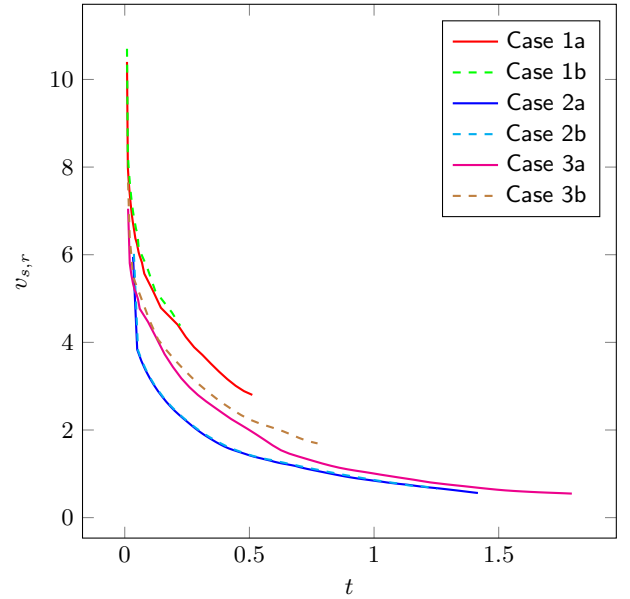


Figure 2. The radial velocity of the liquid sheets ejected from the droplet as function of time. $t = 0$ is defined as the moment of sheet ejection, t_e^R .

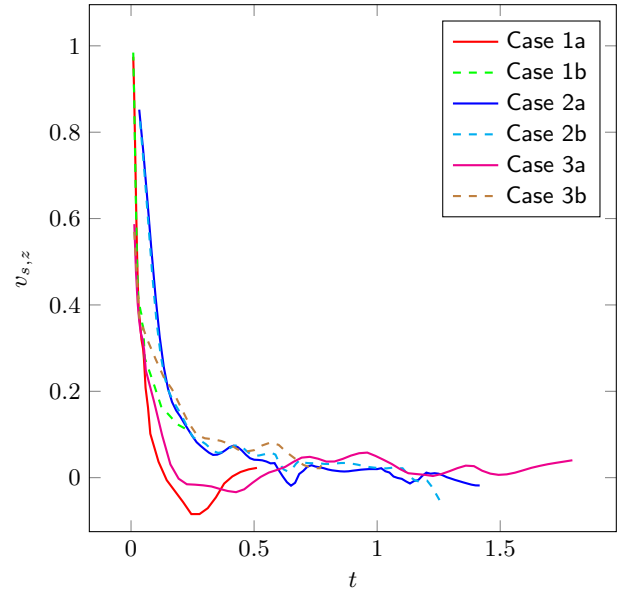


Figure 3. The vertical velocity of the liquid sheets ejected from the droplet as function of time. $t = 0$ is defined as the moment of sheet ejection, t_e^R .

In conclusion, it is found that these simulations support the idea of splashing being a two stage process: first a liquid sheet needs to form, and then this liquid sheet needs to become unstable for a splash to be observed. Also, considering the difference in vertical velocity at different pressures, these simulations are consistent with the idea that a liquid sheet experiences a lift force due to gas flow around it, and that at lower pressure less lift

is generated. Comparing liquid sheet ejection times and velocities found in the simulations to the theories of Mandre and Brenner [11] and Riboux and Gordillo [12], it is found that the theory by Mandre and Brenner accurately predicts liquid sheet ejection velocities and also predicts the right order for the ejection time if the time of first contact with the wall is chosen as the time of impact. The theory by Riboux and Gordillo systematically over-predicts ejection times while under-predicting ejection velocities, which suggests the dewetting criterion needs to be revised. The predicted values for β_R also do not match with the values calculated from the simulations. Last but not least, while as expected, a higher impact velocity is needed to splash an axisymmetric droplet compared to a non-axisymmetric cylinder, all conclusions hold for both cases.



[1] C. W. Hirt and B. D. Nichols, *J. Comput. Phys.* **39**, 201 (1981).

- [2] H. Rusche, *Computational Fluid Dynamics of Dispersed Two-Phase Flows at High Phase Fractions*, Ph.D. thesis, Imperial College (2002).
- [3] J. U. Brackbill, D. B. Kothe, and C. Zemach, *J. Comput. Phys.* **100**, 335 (1992).
- [4] T. Qian, X.-P. Wang, and P. Sheng, *Phys. Rev. E* **68**, 016306 (2003).
- [5] J.-F. Gerbeau and T. Lelievre, *Comput. Methods in Appl. Mech. Eng.* **198**, 644 (2009).
- [6] A. M. P. Boelens and J. J. de Pablo, To be submitted (2015).
- [7] G. K. Batchelor, *An Introduction to Fluid Dynamics*, Cambridge Mathematical Library (Cambridge University Press, 2000).
- [8] OpenCFD Ltd, “OpenFOAM (Version 2.1.1) [Computer software],” (2011).
- [9] S. G. Jennings, *J. Aerosol Sci.* **19**, 159 (1988).
- [10] L. Xu, W. W. Zhang, and S. R. Nagel, *Phys. Rev. Lett.* **94**, 184505 (2005).
- [11] S. Mandre and M. P. Brenner, *J. Fluid Mech.* **690**, 148 (2012).
- [12] G. Riboux and J. M. Gordillo, *Phys. Rev. Lett.* **113**, 024507 (2014).